

## Photovoltaic Performance of Polymers Based on Dithienylthienopyrazines Bearing Thermocleavable Benzoate Esters

Martin Helgesen\* and Frederik C. Krebs

Risø National Laboratory for Sustainable Energy, Technical University of Denmark, Frederiksborgvej 399, DK-4000 Roskilde, Denmark

Received November 10, 2009; Revised Manuscript Received December 17, 2009

**ABSTRACT:** Thermocleavable low-band-gap polymers based on dithienylthienopyrazines were prepared and copolymerized with different donor units like dialkoxybenzene, fluorene, thiophene, and cyclopentadithiophene (CPDT) using both Stille and Suzuki cross-coupling reactions. In the solid state the band gaps are in the range of 1.17–1.37 eV. The polymers were explored as donor materials in bulk heterojunction solar cells together with PCBM as the acceptor material where they were shown to exhibit a photoresponse in the full absorption range up to 900 nm and power conversion efficiencies of up to 1.21% under 1 sun irradiation. A red shift of the absorption edge on going from solution to the solid film was observed for all the polymers. Thermogravimetric analysis of the polymers in the temperature range from 25 to 500 °C showed a weight loss at just above 200 °C, corresponding to loss of the tertiary ester groups, and a second weight loss above 400 °C, corresponding to loss of CO<sub>2</sub> and decomposition. Upon thermocleavage the power conversion efficiency decreased for all the polymers while the polymer films became insoluble which was desired in the context of multilayer film processing. Thermocleavable low-band-gap materials can potentially offer better light harvesting, better operational stability, and a higher level of permissible processing conditions due to the insolubility of thermocleaved films in all solvents.

### Introduction

Low-band-gap polymers for photovoltaics are designed to match the solar emission spectrum better, which has a maximum in photon flux near 700 nm and an appreciable tail stretching into the infrared region.<sup>1,2</sup> The extended absorption by low-band-gap polymers can potentially increase the power conversion efficiency by absorbing more photons. One approach to designing these materials is by use of alternating electron-rich (donor) and electron-poor (acceptor) units giving rise to a material with a low-energy absorption band that is generally ascribed to a charge transfer band. The absorption can be tuned by adjusting the donor–acceptor strengths, or HOMO–LUMO levels, respectively. For this purpose, polymers with alternating dithiophene and thienopyrazine units have been explored by several groups<sup>3–9</sup> who reports band gaps in the range 1.2–1.6 eV for this type of polymer. In our earlier work,<sup>3</sup> we explored the chemistry of the thienopyrazine-type acceptor moiety to characterize the influence of the substituents and extended  $\pi$ -system on the absorption spectrum. Here we found that adding phenyl groups to the dithienylthienopyrazine system caused a red shift of the lowest energy absorption band with up to 50 nm, presumably due to the more extended conjugation. In addition, polymers based on fused aromatic thienopyrazine units can reduce the band gap even further caused by a more planar backbone between repeating units.<sup>3,5</sup> Low-band-gap polymers based on dithienylthienopyrazine in blends with soluble methanofullerenes have shown high power conversion efficiencies (2.2%)<sup>9</sup> and an extended photoresponse up to 900 nm,<sup>7</sup> indicating that these materials are promising for photovoltaic applications.

There has been a recent interest in the operational stability of polymer solar cells and more importantly on the understanding

of why devices and materials break down.<sup>10</sup> By using time-of-flight secondary ion mass spectrometry (TOF-SIMS)<sup>11</sup> and isotopic labeling (<sup>18</sup>O<sub>2</sub> and H<sub>2</sub><sup>18</sup>O), the main finding is that oxygen and water diffuse into the various layers of the solar cell, react with the bulk of the materials and the interfaces, and thus degrade the solar cell and device performance.<sup>12–18</sup> Moreover, photodegradation studies of both MDMO-PPV and P3HT under illumination in the presence and absence of oxygen<sup>19–22</sup> have shown that widely different mechanisms are in play. Illumination of MDMO-PPV in the absence of oxygen suggests that absorption of UV–vis light by MDMO-PPV can induce the homolytic scission of the O–CH<sub>2</sub> bond. The generated radicals may react with the vinylene groups, which lead to loss of conjugation, or undergo photo-Fries rearrangement. Furthermore, different photochemical mechanisms have been shown to be in play, the photochemical instability of P3HT has been suggested to be mainly due to the hexyl side chains, and it has been predicted that the photochemical stability of native polythiophene should be significantly longer. Taking the above-mentioned issues into consideration, one could explore the many possibilities in employing a conjugated material that is reached either through a precursor route or through a route where side chains are removed post film formation. This can be realized with the use of thermocleavable side chains. The side chains provide solubility in organic solvents and allow film formation via solution processing. Subsequently, they can be removed by heating in a postprocessing step forming a harder insoluble material where diffusion phenomena are slowed down and in addition the photochemical reactions associated with the side chains are avoided. Ideally, the thermocleavage of the side chains leads to a high-*T<sub>g</sub>* material, characterized by its high glass transition temperature, which has been demonstrated to strongly suppress morphological changes in high-*T<sub>g</sub>* PPV:PCBM active layers that leads to high thermal stability of the photovoltaic characteristics.<sup>23</sup> Because of a high

\*Corresponding author. E-mail: manp@risoe.dtu.dk.

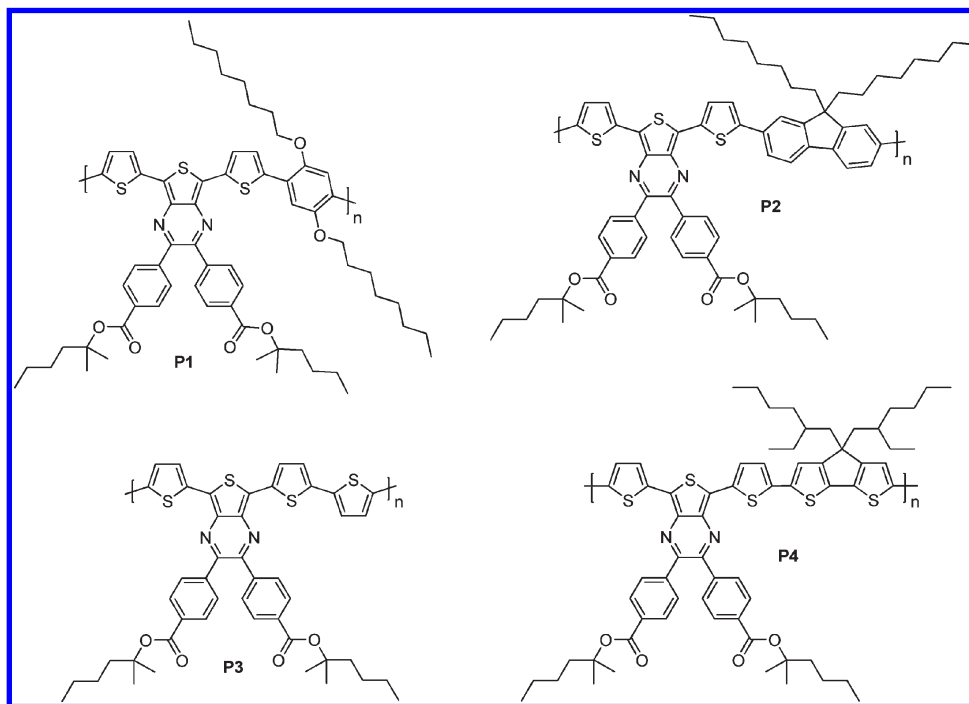


**Figure 1.** Low-band-gap polymers based on dithienylthienopyrazine alternating with different donor segments.

glass transition temperature, the active layer forms a more rigid and stable morphology which limit the possible migration and segregation of the PCBM molecules leading to a more stable active layer and consequently to a more stable photovoltaic behavior.<sup>23</sup> Alternative routes to polymer materials for polymer solar cells without side chains are precursor routes such as the dithiocarbamate route.<sup>24–28</sup> Lifetimes over 10 000 h have been reported for solar cells based on the thermocleavable polymer poly-3-(2-methylhexan-2-yl)oxycarbonylbithiophene (P3MHOCT) and C<sub>60</sub> after thermal elimination of the solubilizing groups which transforms P3MHOCT into the more rigid and insoluble poly-3-carboxydithiophene (P3CT).<sup>17,29</sup>

In spite of the more complex synthetic chemistry and materials handling requirements for thermocleavable materials, the motivations for exploring those in the context of polymer solar cells include improvement of morphological, interface, and photochemical stability, improvement of the chromophore density in the device film, and significant advantages in terms of processing (solubility/insolubility switching). Thermocleavable materials remain inferior to the current state of the art in terms of power conversion efficiency while recent progress have shown power conversion efficiencies approaching 2%. It is likely that thermocleavable materials can be improved at least to the level of the current state-of-the-art pending the same investment in optimization as materials such as P3HT has received.

Herein we report our efforts in this direction through the synthesis of a series of alternating thermocleavable low-band-gap polymers and their photovoltaic performance in blends with [6,6]-phenyl C<sub>61</sub> butyric acid methyl ester (PCBM). The materials are copolymers based on dithienylthienopyrazine, bearing thermocleavable benzoate esters on the pyrazine ring, alternating with different donor segments, i.e., dialkoxybenzene, fluorene, thio-phenyl, and cyclopentadithiophene (CPDT) (Figure 1). The effects of the different donor segments on the photovoltaic performance of the polymers in blends with [60]PCBM with and without thermal treatment are presented. The alkyl benzoate ester groups make the polymer soluble in organic solvents and allow for film formation. Subsequently, they can be removed by heating in a postprocessing step forming the free acid and a volatile alkene.

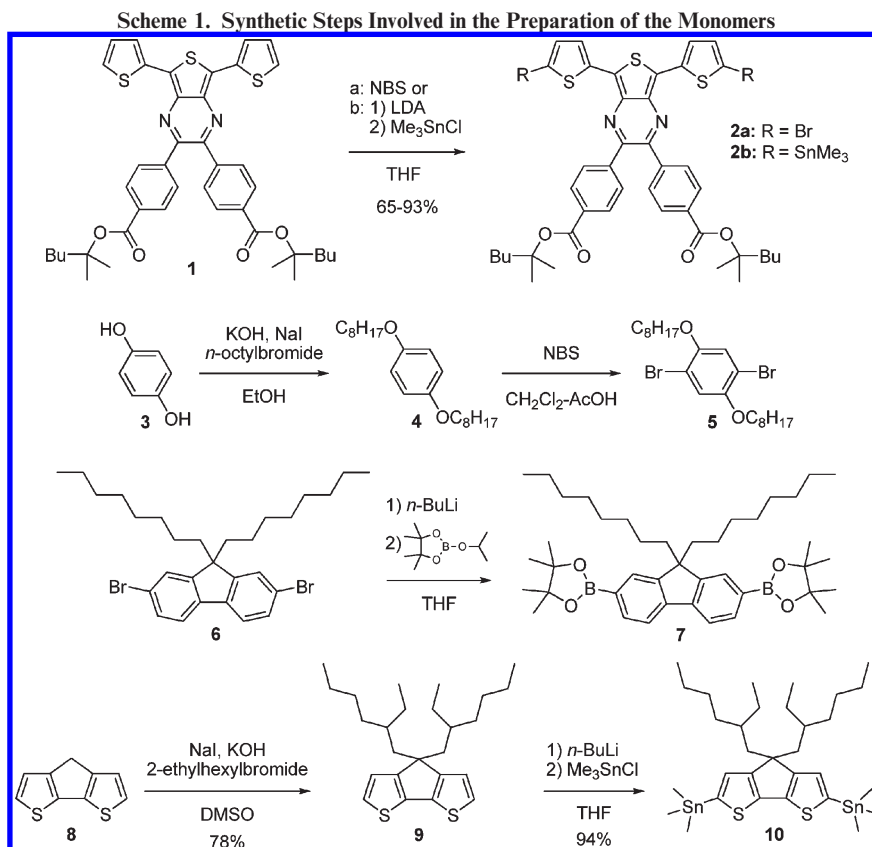
## Experimental Section

Synthetic procedures for synthesis of monomers and polymers according to Schemes 1 and 2 and their characterization data (including <sup>1</sup>H NMR and <sup>13</sup>C NMR) are described in detail in the Supporting Information together with general experimental details.

**Polymer Solar Cell Fabrication and Analysis.** Photovoltaic devices were made by spin-coating PEDOT:PSS (Aldrich, 1.3 wt % aqueous solution) onto precleaned, patterned indium tin oxide (ITO) substrates (9–15 Ω per square) (LumTec) followed by annealing at 140 °C for 5 min. The active layer was deposited, in a glovebox, by spin-coating a blend of the polymer and [60]PCBM dissolved in *o*-dichlorobenzene (40 mg/mL). After a thermal treatment (see Table 2) the counter electrode of aluminum was deposited by vacuum evaporation at  $(2–3) \times 10^{-6}$  mbar. The active area of the cells was 0.5 cm<sup>2</sup>. *I*–*V* characteristics were measured under AM1.5G corresponding to 74.3 mW/cm<sup>2</sup> white light from a multiwavelength high-power LED array using a Keithley 2400 source meter. IPCE spectra were recorded on the same solar test platform with the LED-based illumination system.

## Results and Discussion

**Synthesis.** The synthetic steps involved in the preparation of the monomers **2a**, **2b**, **5**, **7**, and **10** are outlined in Scheme 1. Monomer **1** was functionalized by NBS bromination and by deprotonation using lithium diisopropylamine (LDA) followed by treatment with trimethyltin chloride. This afforded **2a**<sup>30</sup> and **2b**<sup>31</sup> to be used in Suzuki- and Stille-type copolymerizations. According to a literature procedure,<sup>32</sup> monomer **5** can be synthesized in good yield starting with a standard alkylation of hydroquinone (**3**) followed by bromination of **4** with NBS. The diboronic acid pinacol ester **7** is prepared by lithiation of readily available 2,7-dibromo-9,9-dioctylfluorene (**6**) followed by addition of 2-isopropoxy-4,4,5,5-tetramethyl-1,3,2-dioxaborolane.<sup>33</sup> The synthetic route to **10**<sup>34</sup> initiates with a deprotonation of 4*H*-cyclopenta-[2,1-*b*:3,4-*b'*]-dithiophene (**8**) and a subsequent alkylation which affords **9** in good yield. Deprotonation of **9** using



<sup>a</sup>Y = **5**, **7**, **10**, and 2,5-bis(trimethylstannyl)thiophene. (i) Stille coupling using Pd<sub>2</sub>dba<sub>3</sub> and tri-*o*-tolylphosphine. (ii) Suzuki coupling using Pd<sub>2</sub>dba<sub>3</sub>, tri-*o*-tolylphosphine and Cs<sub>2</sub>CO<sub>3</sub>.

*n*-butyllithium followed by treatment with trimethyltin chloride affords monomer **10**.

Copolymerizations leading to the final polymers **P1–P4** are presented in Scheme 2. Copolymerization of **2b** via Stille coupling, using the catalyst system Pd<sub>2</sub>dba<sub>3</sub>/tri-*o*-tolylphosphine, with **5** gave polymer **P1** in 77% yield as a dark brown solid ( $M_w = 7$  kg/mol, PDI = 1.9). Coupling of **2a** with **7** was performed with a Suzuki-type copolymerization reaction using Pd<sub>2</sub>dba<sub>3</sub>/tri-*o*-tolylphosphine as a catalyst and caesium carbonate as a base. The polymer **P2** was afforded in 90% yield as a green solid with a molecular weight ( $M_w$ ) of 42.3 kg/mol and a polydispersity (PDI) of 3. Using the same conditions as for the preparation of **P1**, copolymerization of **2a** via Stille coupling with 2,5-bis(trimethylstannyl)thiophene and the cyclopentadithiophene **10** gave polymer **P3** and **P4** as dark green solids in 92–93% yield. All the polymers were isolated in good yields and are soluble in organic solvents such as chloroform and toluene at room temperature.

**Thermal Behavior.** The thermal behavior of the thermocleavable polymers was investigated by thermogravimetric analysis (TGA). The sample holders were carefully weighed and the samples introduced. TGA was then carried out using heating rate of 10 °C min<sup>-1</sup>. TGA of **P1–P4** are shown in Figure 2 and indicates that the tertiary ester starts to eliminate around 200 °C, in agreement with earlier results.<sup>30</sup> The second loss peak at ~400 °C that corresponds to loss of CO<sub>2</sub><sup>30</sup> (not prior to decomposition) can only be observed for **P3** because a greater weight loss for **P1**, **P2**, and **P4** is showing in the same temperature range. The observed value for this loss peak is ~20%, which corresponds to loss of the alkyl chains on the donor units: dialkoxybenzene, fluorene, and CPDT. The same precursor film prepared by standard solution processing of **P1–P4** can give access to two chemically different thin films, as shown in Figure 3.

**Optical Properties.** The absorption spectra for the polymers in chloroform solution are shown in Figure 4a. The copolymers **P1–P4** based on dithienylthienopyrazine does

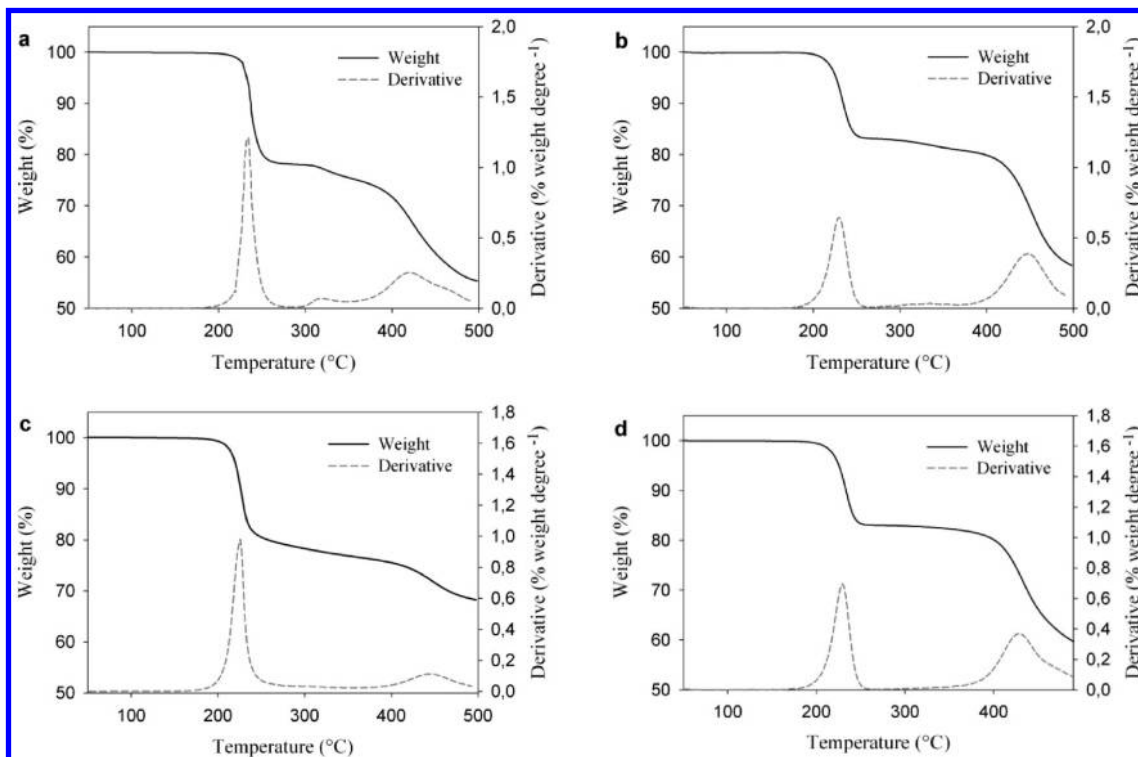


**Figure 2.** (a) TGA of **P1**, (b) TGA of **P2**, (c) TGA of **P3**, and (d) TGA of **P4** in the temperature range 50–500 °C. The data were recorded at 10 °C min<sup>-1</sup> under an argon atmosphere. A derivative weight loss curve has been included to tell the point at which weight loss is most apparent.

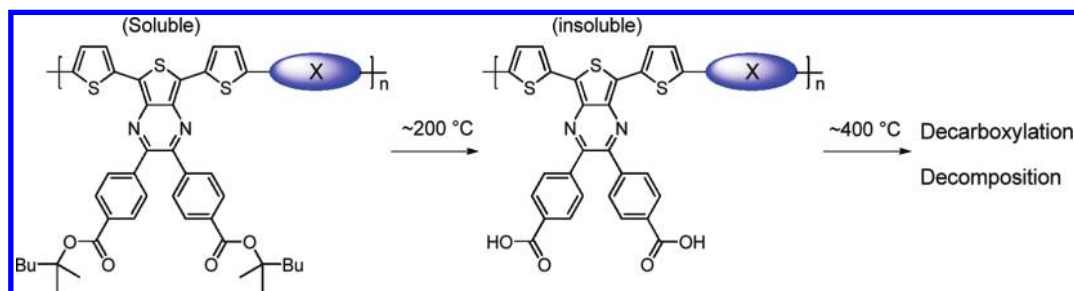


**Figure 3.** Possible chemical transitions of **P1–P4**.

indeed show a considerable spectral coverage of the solar spectrum which is varied with the different donor units. The optical band gaps, defined by the onset of absorption, are ranging from 1.22 to 1.50 eV (Table 1), which is much smaller than that of poly(3-hexylthiophene) (P3HT) homopolymer ( $E_g \sim 1.9\text{--}2.1$  eV). This supports the idea that the internal charge-transfer interaction between donor and acceptor moieties in donor–acceptor copolymers is an efficient method to lower the band gap of conjugated polymers. Partial aggregation of **P1** in solution gives it the lowest optical band gap with an onset at 1015 nm. **P2** has a somewhat higher band gap of 1.5 eV because of the decreased donor strength of the fluorene unit (high degree of aromaticity) which reduce conjugation in the polymer backbone.

Three alternating thiophene units provide **P3** with a band gap of 1.3 eV in solution. Further extending the thiophene content by incorporating CPDT lowers the band gap to 1.27 eV (**P4**). Despite the improved donor character of the CPDT unit, caused by its planarity and electron-donating alkyl chains, **P3** and **P4** have rather similar band gaps though the absorption maxima ( $\lambda_{\max}$ ) of **P3** is blue-shifted compared to **P4**. The thin film absorption spectra for polymers **P1–P4** are shown in Figure 4b. The optical band gaps are ranging

from 1.17 to 1.37 eV where only **P2** shows a significant decrease compared to in solution (Table 1). The polymers **P1** and **P2** have absorption maxima in the range from 665 to 745 nm in chloroform solution, and these are red-shifted further to 710–845 nm when in a solid film (Table 1), indicating significant interchain association in the solid state. In addition,  $\lambda_{\max}$  for **P2** is red-shifted with 50–95 nm compared to corresponding polymers without the thermocleavable side chains.<sup>4,9</sup> **P3** reveals a shoulder around 800 nm in solution, and the same, but weaker, vibronic fine structure remains in the solid state. **P4** also reveals a shoulder in solution around 830 nm, but in the solid state the absorption band has broadened, caused by intermolecular interactions, and the vibronic fine structure has disappeared. Upon annealing the films only **P3** and **P4** shows a significant change in the absorption spectra (Figure 5). Upon thermocleavage of the films by heating them at 250 °C for 1 min a color change from olive green to a more brownish color is observed. The associated changes in the absorption spectrum are a less intense low-energy absorption band and a smaller band gap which is reduced to 1.23 eV for **P3** and 1.18 eV for **P4**. There may be several explanations for the lower absorption intensity. First, the associated change in film thickness,

and secondly, the dielectric constant may lead to changes in the reflection phenomena that also contribute to the intensities in the observed absorption spectrum for a solid film in transmission geometry. Thirdly, the intensity of absorption quite often decreases as the band gap is lowered. After the short thermal treatment the films maintained the optical quality and were insoluble in organic solvents.

**Photovoltaic Performance.** Bulk heterojunction solar cells with an active area of  $0.5 \text{ cm}^2$  were prepared on an indium tin oxide (ITO) covered glass substrate, using conventional device architecture. A thin layer of poly(3,4-ethylenedioxythiophene)–poly(styrenesulfonate) (PEDOT–PSS) was spin-coated on top of the ITO coating followed by spin-coating of the active layer. The active layer contained a blend of the respective polymer and [60]PCBM.

After spin-coating of the active layer the devices were either processed directly into a solar cell by evaporation of aluminum as back electrode or subjected to a thermal treatment at the temperature of thermocleavage immediately before evaporation of the back electrode. The obtained current–voltage curves are presented in Figure 6 which shows the current–voltage characteristics of the polymer:PCBM solar cells measured under  $74.3 \text{ mW/cm}^2$  white light. The unannealed devices based on **P1**, with the lowest band

gap (1.15 eV), and PCBM had low open-circuit voltages ( $V_{oc}$ ) of 0.36 V, moderate fill factors (FF) of 0.40, and current densities ( $J_{sc}$ ) of  $1.82 \text{ mA/cm}^2$ . This resulted in power conversion efficiencies of up to 0.35% (Table 2). Devices based on the fluorine-coupled polymer **P2** and PCBM showed a somewhat higher  $V_{oc}$  up to 0.65 V (Figure 6a) as expected from earlier reports<sup>9</sup> with a similar system. **P2** provides a decent FF of 0.44, but the low current density ( $1.41 \text{ mA/cm}^2$ ) limits the performance to 0.54%. Changing the polymer backbone to be a complete thiophene segment raises the  $J_{sc}$  up to  $2.22 \text{ mA/cm}^2$  for **P3**:PCBM devices. The  $V_{oc}$  was 0.5 V, and together with a FF of 0.38 the devices had a power conversion efficiency up to 0.57%. Solar cells based on **P4**:PCBM exhibits the best performance with the highest current density of  $3.20 \text{ mA/cm}^2$  and a good fill factor of 0.51. Together with an open-circuit voltage of 0.55 V, the power conversion efficiency sets to 1.21%. The somewhat higher  $J_{sc}$  obtained with **P4** is also reflected in the incident photon to current efficiency (IPCE) which reaches an average IPCE of 17% with a photoresponse up to 900 nm (Figure 7a). In contrast, **P1–P3** have an average IPCE in the range 7–8% but also extends up to 900 nm, except **P2** in agreement with the absorption spectra (Figure 4b). Despite the extended photoresponse of **P1–P4**, IPCE is inferior compared to the state of the art system P3HT:PCBM (Table 2) which may be explained by limited exciton dissociation at the

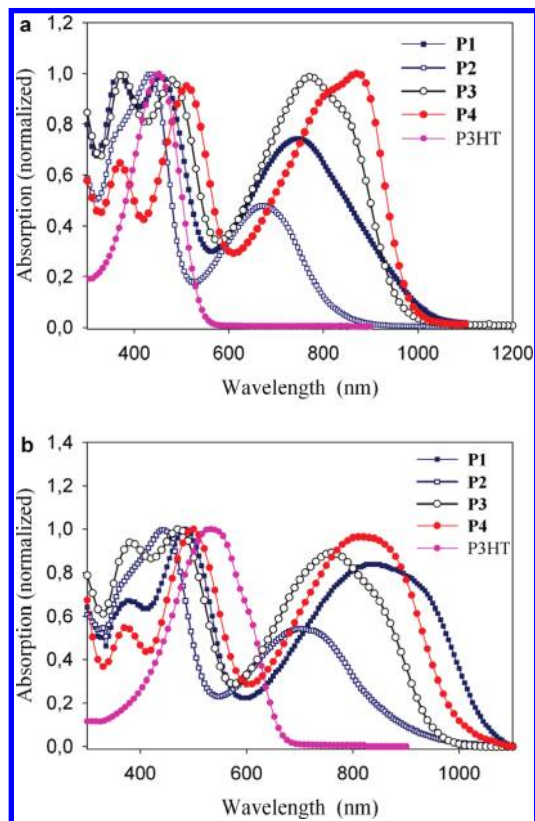


**Figure 4.** (a) UV–vis absorption spectra of the polymers **P1–P4** in chloroform solution and (b) in thin film. P3HT in chloroform solution and in thin film is also shown for comparison.

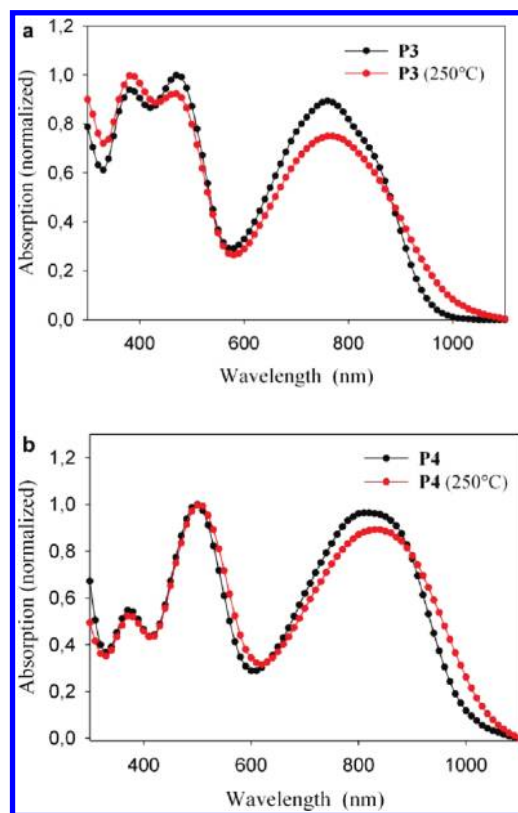


**Figure 5.** (a) UV–vis absorption spectra of **P3** and (b) **P4** in thin film before and after annealing for 1 min.

**Table 1. GPC and Spectroscopic Data for Polymers **P1–P4****

polymer	$M_w$ (g/mol)	PDI	solution				film		
			$\alpha(\lambda_{max})$ (L/(g cm))	$\lambda_{max}$ (nm)	$\lambda_{onset}$ (nm)	$E_g$ (eV)	$\lambda_{max}$ (nm)	$\lambda_{onset}$ (nm)	$E_g$ (eV)
<b>P1</b>	7 000	1.9	16	745	1015	1.22	845	1057	1.17
<b>P2</b>	42 300	3.0	18	665	824	1.50	710	906	1.37
<b>P3</b>	39 400	1.9	23	770	955	1.30	760	955	1.30
<b>P4</b>	363 000	4.8	29	868	980	1.27	825	1002	1.24

polymer–PCBM interface. However for **P4**, the generated charge carriers seem to be extracted relatively efficiently as is indicated by a rather good fill factor of 0.51.  $J$ – $V$  curves of the polymer:PCBM solar cells after a thermal treatment are shown in Figure 6b, and a general observation is that the performance drops after the thermocleavage. Table 2 shows a large drop in the current density for all polymers after thermocleavage together with minor drops in the  $V_{oc}$  and FF. The drop in performance is also reflected in the IPCE which is lower at all wavelengths compared to the unannealed devices (Figure 7b).

**Morphology.** The **P3**:PCBM and **P4**:PCBM device films annealed at different temperatures, as measured by atomic force microscopy (AFM), are shown in Figure 8. AFM reveals changes in the surface topography of the films and generally gives a good first insight into morphology of the active layer.<sup>35</sup> All films shows a significant roughness with a peak-to-valley difference around 15–20 nm. Comparing the films before and after thermocleavage ( $\sim 200$  °C) reveals that the domain sizes increases to features with dimensions larger

than 100 nm which indicate extensive phase segregation of the polymer and PCBM upon annealing at high temperatures. Moreover, Figure 8c,g indicates that phase segregation commence prior to thermal cleavage of the tertiary esters. The reduced current densities of the polymer:PCBM devices after thermocleavage might be a direct consequence of the changed morphology which is possibly limiting charge carrier generation (reduced number of excitons reach the interface) and transport to the electrodes (insufficient percolating pathways). The drop in the current density after thermocleavage to the free carboxylic acid has been observed before for polymers where the thermocleavable ester resides on a thiophene unit. These polymers can undergo further transformation into the native system by decarboxylation which leads to a significant improvement in performance due to an increase in mainly the current density.<sup>36,37</sup> For the materials reported here heating to 300 °C resulted in significantly poorer performance. As measured by AFM, one possible explanation is that the morphology changes undesirably for this class of materials at the high temperatures, and further work on understanding the complex interplay between the

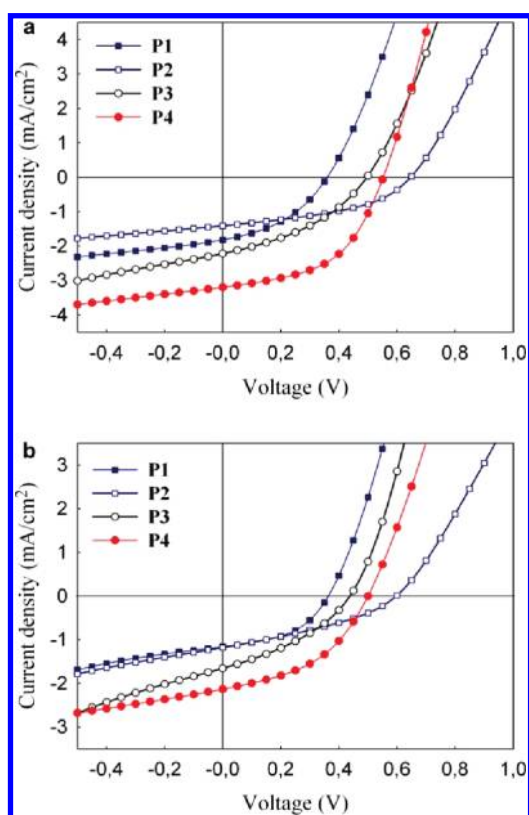


**Figure 6.** (a)  $J$ – $V$  characteristics of the **P1**:PCBM, **P2**:PCBM, **P3**:PCBM, and **P4**:PCBM solar cells measured under  $74.3 \text{ mW/cm}^2$  white light before and (b) after a thermal treatment (see Table 2).

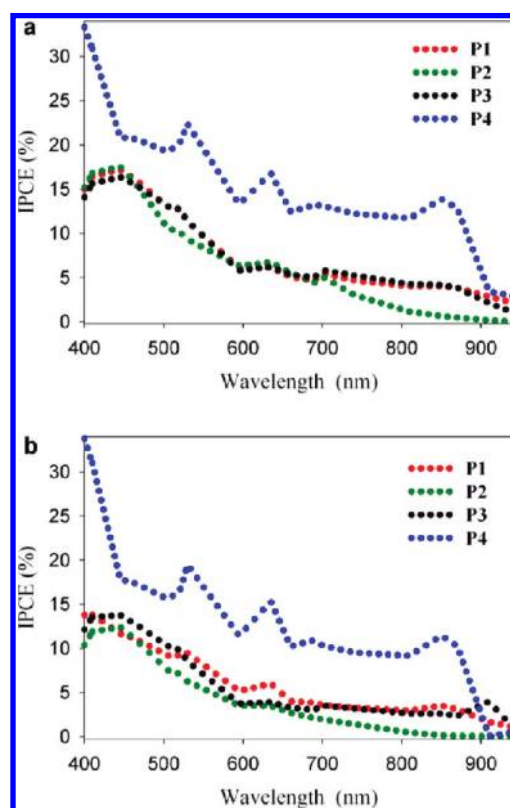


**Figure 7.** (a) IPCE of polymer:PCBM solar cells before and (b) after a thermal treatment.

**Table 2. Photovoltaic Performance of Devices Based on Blends of Polymer and PCBM**

polymer	polymer:PCBM (w/w ratio)	thermal treatment (°C)	$V_{oc}$ (V)	$J_{sc}$ ( $\text{mA/cm}^2$ )	FF	$\eta$ (%)
<b>P1</b>	1:2		0.36	1.82	0.40	0.35
<b>P1</b>	1:2	250 <sup>a</sup>	0.36	1.16	0.47	0.27
<b>P2</b>	1:3		0.65	1.41	0.44	0.54
<b>P2</b>	1:3	250 <sup>a</sup>	0.60	1.18	0.35	0.33
<b>P3</b>	1:4		0.50	2.22	0.38	0.57
<b>P3</b>	1:4	230 <sup>a</sup>	0.44	1.66	0.36	0.35
<b>P4</b>	1:3		0.55	3.20	0.51	1.21
<b>P4</b>	1:3	225 <sup>a</sup>	0.50	2.13	0.45	0.64
<b>P3HT</b>	1:1	150 <sup>b</sup>	0.62	7.69	0.48	2.3 <sup>c</sup>

<sup>a</sup> Annealed for 30 s. <sup>b</sup> Annealed for 5 min. <sup>c</sup> Typical PCE reached at Risø DTU with commercially available regioregular P3HT in the same device geometry.

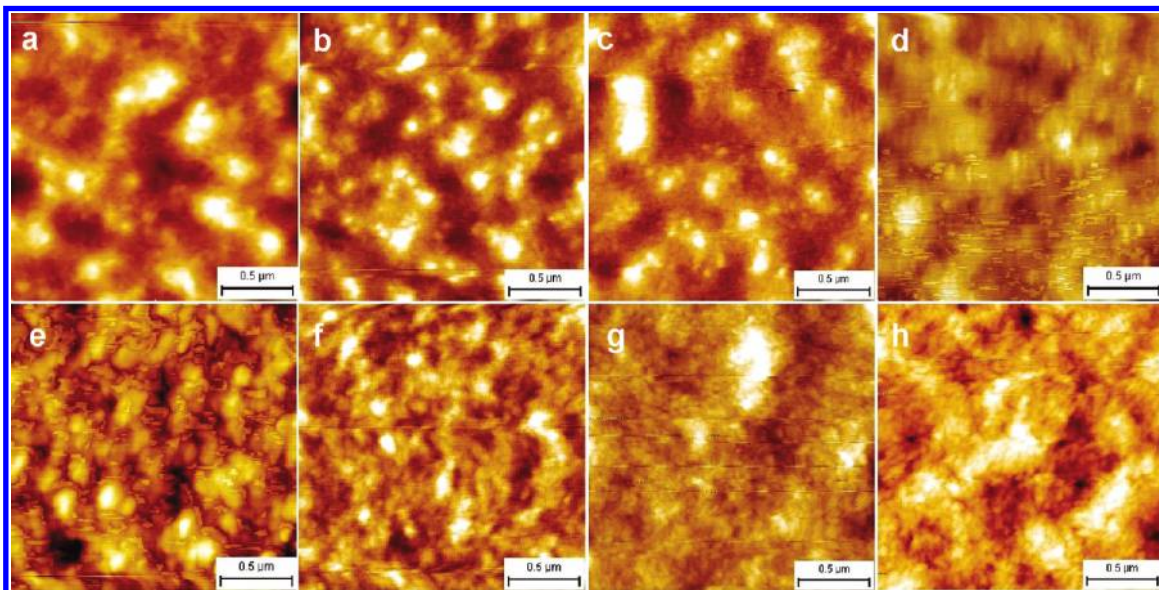


**Figure 8.** AFM topography images ( $2\ \mu\text{m} \times 2\ \mu\text{m}$ ) of solar cells based on blends of PCBM and (a) **P3** unannealed, height scale is 20 nm; (b) **P3** annealed at 150 °C, height scale is 15 nm; (c) **P3** annealed at 180 °C, height scale is 15 nm; (d) **P3** annealed at 230 °C, height scale is 15 nm; (e) **P4** unannealed, height scale is 15 nm; (f) **P4** annealed at 150 °C, height scale is 15 nm; (g) **P4** annealed at 180 °C, height scale is 15 nm; (h) **P4** annealed at 225 °C, height scale is 15 nm.

changes in morphology as a result of thermocleavage is warranted. This points to the importance of the difference between the temperature where changes in morphology take place and the temperature at which thermocleavage takes place. It is likely that the few examples where similar or better performance was obtained after thermocleavage of the film represent cases where the morphology does not change before thermocleavage.

## Conclusion

A series of new thermocleavable low-band-gap polymers based on dithienylthienopyrazine, bearing thermocleavable benzoate esters on the pyrazine ring, alternating with different donor segments (including dialkoxybenzene, fluorene, thiophene, and CPDT) have been synthesized. The solubilizing benzoate ester groups are thermocleavable around 200 °C where a volatile alkene is eliminated, leaving the polymer component more rigid. Furthermore, it was found that no decarboxylation takes place prior to decomposition at  $\sim 400$  °C where a greater weight loss for **P1**, **P2**, and **P4** is observed in the same temperature range which corresponds to loss of the alkyl chains on the donor units: dialkoxybenzene, fluorene, and CPDT. The four polymers optical properties and photovoltaic performance in blends with PCBM have been investigated. In chloroform solution the polymers had optical band gaps ranging from 1.22 to 1.50 eV. The optical band gaps are lowered to 1.17–1.37 eV in thin film, showing a considerable spectral coverage of the solar emission spectrum. Furthermore, polymers **P3** and **P4** showed a less intense low-energy absorption band and a smaller band gap after annealing the film for 1 min. The best performing polymer in a bulk heterojunction solar cell was **P4** with  $J_{\text{sc}} = 3.20\ \text{mA}/\text{cm}^2$ ,  $V_{\text{oc}} = 0.55\ \text{V}$ ,  $\text{FF} = 0.51$ , and  $\eta = 1.21\%$ . Devices generally performed worse after thermocleavage due to a drop in mainly the current density giving power conversion efficiencies up to 0.64% for **P4**:PCBM solar cells. The drop in performance after thermocleavage can be linked to extensive phase segregation of the polymer and PCBM upon annealing as measured by AFM. We finally conclude that the interplay between temperature, morphology, and film chemistry needs to be understood before efficient thermocleavable materials can be optimally designed.

**Acknowledgment.** This work was supported by the Danish Strategic Research Council (DSF 2104-05-0052 and 2104-07-0022).

**Supporting Information Available:** General procedures and characterization data including NMR spectra; experimental procedures for the synthesis of the monomers and polymers according to Schemes 1 and 2. This material is available free of charge via the Internet at <http://pubs.acs.org>.

## References and Notes

- Bundgaard, E.; Krebs, F. C. *Sol. Energy Mater. Sol. Cells* **2007**, *91*, 954–985.
- Kroon, R.; Lenes, M.; Hummelen, J. C.; Blom, P. W. M.; de Boer, B. *Polym. Rev.* **2008**, *48*, 531–582.
- Petersen, M. H.; Hagemann, O.; Nielsen, K. T.; Jørgensen, M.; Krebs, F. C. *Sol. Energy Mater. Sol. Cells* **2007**, *91*, 996–1009.
- Zhang, F. L.; Perzon, E.; Wang, X. J.; Mammo, W.; Andersson, M. R.; Inganäs, O. *Adv. Funct. Mater.* **2005**, *15*, 745–750.
- Mondal, R.; Miyaki, N.; Becerril, H. A.; Norton, J. E.; Parmer, J.; Mayer, A. C.; Tang, M. L.; Brédas, J.-L.; McGehee, M. D.; Bao, Z. *Chem. Mater.* **2009**, *21*, 3618–3628.
- Campos, L. M.; Tontcheva, A.; Gunes, S.; Sonmez, G.; Neugebauer, H.; Sariciftci, N. S.; Wudl, F. *Chem. Mater.* **2005**, *17*, 4031–4033.
- Zoombelt, A. P.; Gilot, J.; Wienk, M. M.; Janssen, R. A. J. *Chem. Mater.* **2009**, *21*, 1663–1669.
- Wienk, M. M.; Turbiez, M. G. R.; Struijk, M. P.; Fonrodona, M.; Janssen, R. A. J. *Appl. Phys. Lett.* **2006**, *88*, 153511.
- Zhang, F. L.; Mammo, W.; Andersson, L. M.; Admassie, S.; Andersson, M. R.; Inganäs, L.; Admassie, S.; Andersson, M. R.; Inganäs, O. *Adv. Mater.* **2006**, *18*, 2169–2173.
- Jørgensen, M.; Norrman, K.; Krebs, F. C. *Sol. Energy Mater. Sol. Cells* **2008**, *92*, 686–714.
- Norrman, K.; Krebs, F. C. *Surf. Interface Anal.* **2004**, *36*, 1542–1549.
- Norrman, K.; Krebs, F. C. *Sol. Energy Mater. Sol. Cells* **2006**, *90*, 213–227.
- Lira-Cantu, M.; Norrman, K.; Andreasen, J. W.; Krebs, F. C. *Chem. Mater.* **2006**, *18*, 5684–5690.
- Norrman, K.; Larsen, N. B.; Krebs, F. C. *Sol. Energy Mater. Sol. Cells* **2006**, *90*, 2793–2814.
- Alstrup, J.; Norrman, K.; Jørgensen, M.; Krebs, F. C. *Sol. Energy Mater. Sol. Cells* **2006**, *90*, 2777–2792.
- Norrman, K.; Alstrup, J.; Krebs, F. C. *Surf. Interface Anal.* **2006**, *38*, 1302–1310.

- (17) Krebs, F. C.; Norrman, K. *Prog. Photovoltaics* **2007**, *15*, 697–712.
- (18) Norrman, K.; Gevorgyan, S. A.; Krebs, F. C. *ACS Appl. Mater. Interfaces* **2009**, *1*, 102–112.
- (19) Chambon, S.; Rivaton, A.; Gardette, J. L.; Firon, M. *Sol. Energy Mater. Sol. Cells* **2008**, *92*, 785–792.
- (20) Chambon, S.; Manceau, M.; Firon, M.; Cros, S.; Rivaton, A.; Gardette, J.-L. *Polymer* **2008**, *49*, 3288–3294.
- (21) Manceau, M.; Rivaton, A.; Gardette, J.-L. *Macromol. Rapid Commun.* **2008**, *29*, 1823–1827.
- (22) Manceau, M.; Rivaton, A.; Gardette, J.-L.; Guillerez, S.; Lemaître, N. *Polym. Degrad. Stab.* **2009**, *94*, 898–907.
- (23) Bertho, S.; Janssen, G.; Cleij, T. J.; Conings, B.; Moons, W.; Gadisa, A.; D'Haen, J.; Goovaerts, E.; Lutsen, L.; Manca, J.; Vanderzande, D. *Sol. Energy Mater. Sol. Cells* **2008**, *92*, 753–760.
- (24) Henckens, A.; Colladet, K.; Fourier, S.; Cleij, T. J.; Lutsen, L.; Gelan, J.; Vanderzande, D. *Macromolecules* **2005**, *38*, 19–26.
- (25) Nguyen, L. H.; Günes, S.; Neugebauer, H.; Sariciftci, N. S.; Banishoeib, F.; Henckens, A.; Cleij, T. J.; Lutsen, L.; Vanderzande, D. *Sol. Energy Mater. Sol. Cells* **2006**, *90*, 2815–2828.
- (26) Banishoeib, F.; Adriaensens, P.; Berson, S.; Guillerez, S.; Douheret, O.; Manca, J.; Fourier, S.; Cleij, T. J.; Lutsen, L.; Vanderzande, D. *Sol. Energy Mater. Sol. Cells* **2007**, *91*, 1026–1034.
- (27) Banishoeib, F.; Henckens, A.; Fourier, S.; Vanhooyland, G.; Breselge, M.; Manca, J.; Cleij, T. J.; Lutsen, L.; Vanderzande, D.; Nguyen, L. H.; Neugebauer, H.; Sariciftci, N. S. *Thin Solid Films* **2008**, *516*, 3978–3988.
- (28) Giroto, C.; Cheyns, D.; Aernouts, T.; Banishoeib, F.; Lutsen, L.; Cleij, T. J.; Vanderzande, D.; Genoe, J.; Poortmans, J.; Heremans, P. *Org. Electron.* **2008**, *9*, 740–746.
- (29) Krebs, F. C.; Spanggaard, H. *Chem. Mater.* **2005**, *17*, 5235–5237.
- (30) Petersen, M. H.; Gevorgyan, S. A.; Krebs, F. C. *Macromolecules* **2008**, *41*, 8986–8994.
- (31) Hagemann, O.; Bjerring, M.; Nielsen, N. C.; Krebs, F. C. *Sol. Energy Mater. Sol. Cells* **2008**, *92*, 1327–1335.
- (32) Aubert, P. H.; Knipper, M.; Groenendaal, L.; Lutsen, L.; Manca, J.; Vanderzande, D. *Macromolecules* **2004**, *37*, 4087–4098.
- (33) Ranger, M.; Rondeau, D.; Leclerc, M. *Macromolecules* **1997**, *30*, 7686–7691.
- (34) Zhu, Z.; Waller, D.; Gaudiana, R.; Morana, M.; Muhlbacher, D.; Scharber, M.; Brabec, C. *Macromolecules* **2007**, *40*, 1981–1986.
- (35) Yang, X.; Loos, J. *Macromolecules* **2007**, *40*, 1353–1362.
- (36) Gevorgyan, S. A.; Krebs, F. C. *Chem. Mater.* **2008**, *20*, 4386–4390.
- (37) Helgesen, M.; Gevorgyan, S. A.; Krebs, F. C.; Janssen, R. A. J. *Chem. Mater.* **2009**, *21*, 4669–4675.